# Roll dynamics and lateral load transfer estimation in articulated heavy freight vehicles

R Kamnik, F Boettiger and K Hunt

*Proceedings of the Institution of Mechanical Engineers, Part D: Journal of Automobile Engineering* 2003 217: 985
DOI: 10.1243/095440703770383884

# Roll dynamics and lateral load transfer estimation in articulated heavy freight vehicles

**R Kamnik**[1]*, **F Boettiger**[2] and **K Hunt**[1]
[1]University of Glasgow, Department of Mechanical Engineering, Glasgow, UK
[2]DaimlerChrysler, Stuttgart, Germany

**Abstract:** Roll dynamics in heavy freight vehicles is characterized in driving conditions by the lateral load transfer coefficient. The coefficient tracking requires sophisticated measurement systems for assessing the wheels' normal loading. In this paper a new recursive non-linear lateral load transfer estimator employing sensors that are already used on a vehicle in combination with additional units that are not sophisticated for the implementation is described. The proposed algorithm integrates two subsystems—separate estimators for the tractor and the trailer. The first estimator is based on slip information of the driving wheels, while the second estimator fuses the tractor estimation and the modelled trailer dynamics by the extended Kalman filter. The novel approach was evaluated on a sophisticated computer simulator of the Freightliner Century Class tractor semitrailer. The simulation analysis shows that the proposed algorithm provides robust operation and good tracking performance. This approach enables a practical realization of a low-cost solution for the rollover prevention in real heavy freight vehicles.

**Keywords:** truck rollover, lateral load transfer, rollover prediction

## NOTATION

| | |
|---|---|
| $a_y$ | lateral acceleration measured in a trailer-based coordinate system (m/s$^2$) |
| $a_z$ | vertical acceleration measured in a trailer-based coordinate system (m/s$^2$) |
| $A_x$ | longitudinal acceleration expressed in the inertial coordinate system (m/s$^2$) |
| $A_y$ | lateral acceleration expressed in the inertial coordinate system (m/s$^2$) |
| $C_{\phi s}$ | total torsional damping of the suspension (N m s/deg) |
| $F$ | wheel loading (N) |
| $F_{z,\mathrm{l}}$ | vertical load on the left tyres (N) |
| $F_{z,\mathrm{r}}$ | vertical load on the right tyres (N) |
| $F_{z,\mathrm{front}}$ | normal loading of the tractor drive axles (N) |
| $F_{z,\mathrm{rear}}$ | normal loading of the trailer axles (N) |
| $g$ | gravitational acceleration (m/s$^2$) |
| $h_{\mathrm{cg}}$ | height of centre of gravity (c.g.) of the sprung mass above the ground (m) |
| $h_{\mathrm{r}}$ | distance from the sprung mass centre to the roll axis (m) |
| $h_{\mathrm{u}}$ | height of centre of gravity (c.g.) of the unsprung mass above the ground (m) |
| $I_x$ | mass moment of inertia determined according to the trailer longitudinal axis (kg m$^2$) |
| $K_{\phi s}$ | total torsional stiffness of the suspension (N m/deg) |
| $l_{\mathrm{A}i}$ | longitudinal distance from the tractor c.g. to the tractor rear axles (m), $i = 2, 3$ |
| $L$ | tractor or trailer unit wheel base (m) |
| LLT | lateral load transfer coefficient |
| $L_{\mathrm{B,f}}$ | distance from the trailer c.g. to the front supportive point (m) |
| $L_{\mathrm{B,r}}$ | distance from the trailer c.g. to the rear supportive point (m) |
| $m_{\mathrm{s}}$ | weight of the sprung mass (kg) |
| $m_{\mathrm{u}}$ | weight of the unsprung mass (kg) |
| $r_0$ | original wheel radius (m) |
| $s$ | wheel slip |
| $T$ | effective track width (m) |
| $v_{\mathrm{cg}}$ | vehicle c.g. forward velocity (m/s) |
| $v_{\mathrm{R}}$ | tyre rotational equivalent velocity (m/s) |
| $v_{\mathrm{W}}$ | wheel ground contact point velocity (m/s) |
| $z_{\mathrm{r}}$ | distance from the unsprung mass centre to the roll axis (m) |
| $\beta$ | angle between the chassis c.g. coordinate |

*The MS was received on 28 March 2003 and was accepted after revision for publication on 14 July 2003.*
* *Corresponding author: Faculty of Electrical Engineering, Tržaška 25, 1000 Ljubljana, Slovenia.*

| | |
|---|---|
| | system and the wheel ground contact point (rad) |
| $\mu$ | wheel friction coefficient |
| $\phi_s$ | roll angle of the sprung mass (rad) |
| $\phi_u$ | roll angle of the unsprung mass (rad) |
| $\dot{\psi}$ | vehicle yaw angle rate (rad/s) |
| $\omega$ | wheel angular velocity (rad/s) |

**Subscripts**

| | |
|---|---|
| A | tractor unit |
| B | trailer unit |
| front | unit longitudinal frontal side |
| rear | unit longitudinal backward side |
| l | left |
| r | right |
| res | resultant |
| $x$ | longitudinal component |
| $y$ | lateral component |
| $z$ | vertical component |

## 1 INTRODUCTION

Truck rollover is a serious highway safety problem and one that has significant consequences. Heavy freight vehicles have poor rollover limits and are thus prone to rollover accidents. Under normal road conditions the heavy freight vehicle lateral skid would probably not be initialized before the vehicle rolls over. For example, a survey of highway accidents involving heavy freight vehicles in Canada revealed that nearly 77 per cent of rollover accidents occurred on dry pavement and could be classified as manoeuvre-induced rollovers (citation in reference [**1**]). A manoeuvre-induced rollover is primarily attributed to the dynamic roll behaviour of the vehicle while the contributions from the tripping mechanism are absent. This kind of rollover may occur during low-speed cornering and braking or high-speed evasive directional manoeuvres.

A static rollover threshold (SRT) is most often employed to characterize the roll stability of a vehicle. It is defined as 'the level of steady lateral acceleration in $g$'s which the vehicle can sustain without suffering a divergent roll response, i.e. rollover'. If the vehicle is considered as a rigid body acting in a single roll plane there are only two parameters that affect the SRT—the track width and the centre of gravity height [**2**]. While these two parameters are of fundamental importance for any vehicle, a larger number of parameters influences the SRT. The vehicle SRT can be assessed by simulations, but often it is simpler to determine it experimentally [**3**–**6**]. Recently, an on-board system has been developed that estimates the SRT by taking into account the vehicle loading conditions [**7**]. The lateral acceleration limits for most heavy vehicles have been reported to be in the $0.3g$ to $0.7g$ range [**8**].

The SRT, however, is intended to characterize the roll stability of a vehicle under quasi-static conditions. It has been established that different mass units of articulated vehicle combinations demonstrate varying levels of lateral acceleration response in transient steering manoeuvres. Rollover of articulated heavy vehicles in a dynamic directional manoeuvre may thus occur at a lateral acceleration level considerably different from the SRT. Since vehicle dynamics is neglected, the threshold value is usually overestimated.

The dynamic roll instability of a vehicle, in general, can be considered to occur in two different forms: (a) as relative instability or (b) as absolute instability. The vehicle is considered to be in a relatively unstable condition when it cannot remain stable under the action of a constant level of lateral force at its centre of gravity (c.g.) location. The existence of a relative instability in a dynamic manoeuvre does not imply the definite occurrence of an actual rollover. Such relative instability can lead to an actual rollover only if the sustained level of lateral acceleration is attained for a period of time when the absolute instability is reached. The absolute roll instability of the vehicle occurs at tip-over, when the vehicle's centre of mass aligns vertically above the effective contact region of the outer tyres with the road. The existence of a lateral disturbance or perturbation will then lead to an actual rollover of the vehicle.

It has been established that the dynamic roll instabilities in articulated heavy vehicles are initiated at the rearmost of the vehicle with minimal changes in the dynamic response of the tractor [**1**, **9**]. Consequently, the driver often remains unaware of the impeding instability and therefore some form of an early warning to the driver at the onset of potential vehicle rollover could be vital to enhance road safety.

In the literature, potential rollover indicators have been investigated by the help of parametric sensitivity analysis, examining the sensitivity to variations in operating factors. The onset of the rollover was related to the magnitude of lateral acceleration, roll frequency, roll angle and suspension spring deflection [**10**–**12**]. The majority of these parameters are either extremely sensitive to vehicle design and operational factors or require comprehensive instrumentation. Beside the parametric analyses, the roll stability measures were also considered. Regarding the absolute roll instability criterion, a rollover prevention energy reserve (RPER) and a critical sliding velocity (CSV) have been suggested [**13**, **14**]. These measures are commonly utilized for characterization of the vehicle tripped rollover. On the other hand, the lateral load transfer (LLT) coefficient has been defined on the basis of the relative rollover criterion [**12**, **15**]. The relative roll instability is mostly associated with the loss of tyre contact with the road. Although the loss of tyre–road contact may not yield absolute

roll instability, it is considered undesirable in view of the directional stability and control of the vehicle. Accordingly, the LLT coefficient tracking is suggested as a convenient method for dynamic roll behaviour supervision of the vehicle.

The proposed criteria, however, in practical applications, involves on-line measurement of tyre loads in a moving vehicle, which is considered to be rather intricate. To overcome this difficulty, a measure of suspension loads or axle inclination angle was considered as approximators of the LLT coefficient. The work of Rakheja and Piché [**10**] showed that the suspension force ratio may be considered as a load transfer indicator; however, this measure does not provide a reliable indication in the case when the vehicle is equipped with a air-spring suspension. Since the air springs are precharged and usually do not go into tension, the variations in dynamic spring force of the air suspension are thus quite different from those in the leaf-spring type of suspension. On the other hand, when considering the axle roll inclination for assessing the LLT, it was established that the roll angle response of the tractor rear and trailer axles is quite sensitive to the axle loads.

In this paper, a method for on-board and on-line LLT coefficient estimation designed for articulated freight vehicles is proposed. The algorithm performs separate estimations for the tractor and the trailer units. The paper is organized as follows. The first part defines the LLT coefficients for both vehicle units and explains the background of the estimation approaches. The second part describes the evaluation procedure accomplished on a sophisticated heavy freight vehicle simulation model. In the final part the evaluation results are outlined and the performance of the proposed system is discussed.

## 2 LATERAL LOAD TRANSFER COEFFICIENT AS A DYNAMIC ROLL STABILITY MEASURE

The LLT coefficient, in essence, denotes the centre of pressure position (i.e. the vehicle's c.g. vertical projection to the ground) in a vehicle supportive area. The coefficient approaches a unit value when the wheels on one track of all the axles lift off the ground, meaning in fact that the centre of pressure has left the supportive area. The coefficient is calculated as the ratio of the difference between the sum of the right wheel loads and the sum of the left wheel loads, to the sum of all the wheel loads of the axles. The equation denoting the LLT of the vehicle as a whole has the following form:

$$\mathrm{LLT} = \frac{\text{load on left tyres} - \text{load on right tyres}}{\text{total load on all tyres}} \tag{1}$$

In articulated freight vehicles, in general, the tractor front axle employs a relatively soft suspension and supports considerably less load than the tractor drive and trailer axles. Consequently, the front wheel of the tractor may still retain road contact when the roll instability is initialized. Thus the contribution due to the front axle can be neglected. Furthermore, for vehicles with units partly decoupled in a roll, load transfer ratio calculations apply better within the single suspension units. Hence, the LLT coefficients are defined separately for the tractor and the trailer and are denoted by the indexes A and B respectively:

$$\mathrm{LLT_A} = \frac{\sum_{i=1}^{m} (F_{z\mathrm{A}i,\mathrm{l}} - F_{z\mathrm{A}i,\mathrm{r}})}{\sum_{i=1}^{m} (F_{z\mathrm{A}i,\mathrm{l}} + F_{z\mathrm{A}i,\mathrm{r}})} \tag{2}$$

$$\mathrm{LLT_B} = \frac{\sum_{i=1}^{m} (F_{z\mathrm{B}i,\mathrm{l}} - F_{z\mathrm{B}i,\mathrm{r}})}{\sum_{i=1}^{m} (F_{z\mathrm{B}i,\mathrm{l}} + F_{z\mathrm{B}i,\mathrm{r}})} \tag{3}$$

In equations (2) and (3) the parameter $m$ represents the number of axles on which the wheels should lift off the ground. For the tractor, only the drive axles are counted, while for the trailer all the axles are counted. The forces $F$ represent the vertical tyre forces acting on the left or right side of the particular axle (l or r index notation). Since the process of vehicle rollover is supposed to be initiated at the trailer rearward side, the value $\mathrm{LLT_B} = \pm 1$ could be used as an early indication that the relative roll instability condition had been reached. Unfortunately, the requirement for the tyre load assessment makes the LLT coefficient difficult and impractical for implementation.

## 3 NON-LINEAR LATERAL LOAD TRANSFER ESTIMATION METHOD

For the reasons mentioned in the section above, a novel non-linear method is proposed for a lateral load transfer estimation. The method estimates the lateral load transfer for the tractor and the trailer separately. The main idea is to estimate the $\mathrm{LLT_A}$ and $\mathrm{LLT_B}$ coefficients by exploitation of the sensory systems that are already implemented on a vehicle in combination with additional sensors that are not difficult for implementation. Namely, in modern vehicles equipped with ABS (anti-lock braking system) and ASP (Acceleration Slip Regulation) systems, the measurement and estimation of driving parameters are already being performed and obtained signals are available on-board. As additional sensors, only the sensory systems are allowed that can be mounted on a vehicle chassis without intervention into the chassis structure. Such convenient sensors are the single or multiaxis accelerometers and angle rate sensors whose installation requires only the housing installation and wiring.

A conceptual drawing of the proposed lateral load transfer estimation system is presented in Fig. 1. The figure outlines the key components of the estimation system with its required input signals. The estimation algorithms are presented thoroughly in the following text.

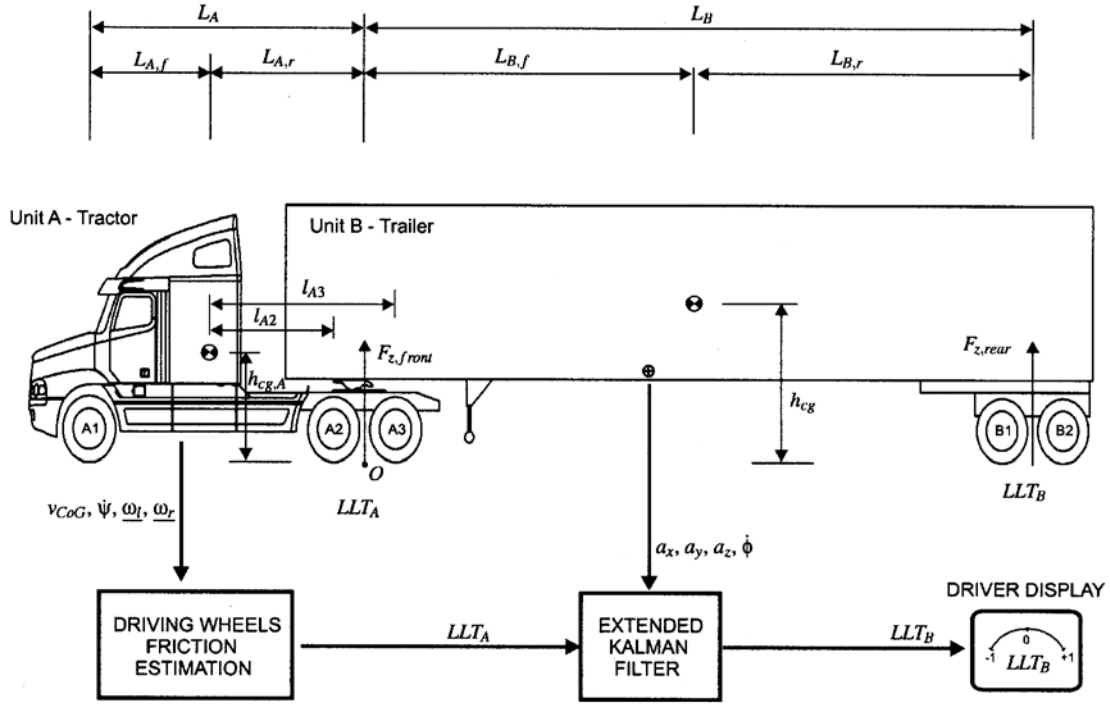


**Fig. 1** Assessment of the tractor and trailer lateral load transfers: a conceptual drawing

### 3.1 Tractor $LLT_A$ coefficient estimation

According to equation (2), the tractor lateral load transfer depends on vertical loading of the tractor driving axles. The function of the driving axles is to support the vertical load and to transfer the engine torque to the wheel longitudinal forces. Since the axle vertical loading cannot be directly estimated, the $LLT_A$ estimation method is based upon the mechanism of differential gearing in driving axles. In each driving axle, the differential gearing ensures the symmetry of the longitudinal wheel forces on the left and the right axle sides. The symmetry is ensured either during straight motion or cornering of the vehicle, and can be described as an equality:

$$F_{x,l} = F_{x,r} \tag{4}$$

where the indices l and r denote the left and right axle sides respectively.

Longitudinal wheel loading is related to vertical wheel loading via the friction, or cohesion, coefficient $\mu_x (F_x = \mu_x F_z)$. In this respect, equation (4) can be rewritten as

$$\mu_{x,l} F_{z,l} = \mu_{x,r} F_{z,r} \tag{5}$$

From the above equality, the $LLT_{Ai}$ coefficient describing the load transfer under a particular driving axle can be derived:

$$LLT_{Ai} = \frac{F_{z,l} - F_{z,r}}{F_{z,l} + F_{z,r}} = \frac{\mu_{x,r} - \mu_{x,l}}{\mu_{x,r} + \mu_{x,l}} \tag{6}$$

In the derived term, the $LLT_{Ai}$ coefficient is still defined on the basis of unmeasurable variables, but the friction behaviour of the wheels can be approximated with a parametric characteristic. The method of Burckhardt (see reference [**16**]) is well known, by which the resultant friction coefficient $\mu_{res}$ in the tyre–road contact is determined on a basis of the resultant wheel slip $s_{res}$:

$$\mu_{res} = f(s_{res}) = c_1 (1 - e^{-c_2 s_{res}}) - c_3 s_{res} \tag{7}$$

In equation (7) the parameter set $c_1$, $c_2$ and $c_3$ correspond to specific road surfaces.

According to the Kamm circle, the longitudinal friction coefficient $\mu_x$ can be related to the resultant friction

$$\mu_x = \mu_{res} \frac{s_x}{s_{res}} = \mu_{res} \frac{s_x}{\sqrt{s_x^2 + s_y^2}} \tag{8}$$

In normal cornering under normal driving conditions it can be assumed that the wheel side slip $s_y$ is near or equal to zero. In such a case, equation (7) approximates the friction conditions well in the longitudinal direction only:

$$\mu_x = f(s_x) = c_1 (1 - e^{-c_2 s_x}) - c_3 s_x \tag{9}$$

Equation (9) is a well suited form of the calculation of the $LLT_{Ai}$ coefficient from equation (6). Namely, the longitudinal wheel slip $s_x$ estimation is practically realizable on a real vehicle. In modern vehicles, which employ the ABS system, the longitudinal slip estimation is already performed and slip information on-board is available for all wheels. Otherwise, the longitudinal wheel slip is defined as

$$s_x = \frac{v_R - v_W}{v_R} \tag{10}$$

where $v_W$ is a wheel ground contact point velocity and $v_R$ is a tyre rotational equivalent velocity. The tyre rotational equivalent velocity is defined by a wheel angular velocity $\omega$ and a tyre radius $r_0$ as

$$v_R = \omega r_0 \tag{11}$$

while the wheel ground contact point velocity for the wheels on rear axles can be estimated from the known vehicle c.g. forward velocity $v_{cg}$, vehicle yaw angle rate $\dot{\psi}$ and vehicle geometry as

$$v_{W,l} = v_{cg} - \dot{\psi}\left(\frac{T}{2} + l_{Ai}\beta\right)$$
$$v_{W,r} = v_{cg} + \dot{\psi}\left(\frac{T}{2} - l_{Ai}\beta\right) \tag{12}$$

In equations (12), $T$ stands for track width, $\beta$ for the angle between the chassis c.g. coordinate system and wheel ground contact point, while $l_{Ai}$ stands for the longitudinal distance from the tractor c.g. to the rear axle. The index $i$ with values of 2 or 3 denotes the first or second tractor driving axle.

Estimation of the wheel longitudinal slip on each axle side and transformation to the friction coefficient according to equation (9) enables the lateral load transfer estimation for the particular driving axle according to equation (6). The lateral load transfer for the whole tractor unit $LLT_A$ is then determined as an averaged sum of the lateral load transfers of both driving axles:

$$LLT_A = \frac{1}{2}\sum_{i=2}^{3} LLT_{Ai} \tag{13}$$

### 3.2 Trailer $LLT_B$ coefficient estimation

Lateral load transfer on the trailer unit in nature differs from the lateral load transfer of the tractor unit. It differs in phase and amplitude with regards to the loading conditions and the roll dynamics. In this section, the trailer unit is considered as a lumped mass and its dynamic behaviour described by simple dynamic equations. On the basis of the modelled dynamics and the known tractor lateral load transfer, the lateral load transfer of the trailer axles is estimated by means of the extended Kalman filter algorithm. Kalman filtering is a common approach in automotive engineering employed for inaccessible vehicle states estimation [**17**–**20**]. The $LLT_B$ coefficient is in this way determined with regards to the modelled dynamics, the known $LLT_A$ coefficient, trailer unit acceleration and its roll rate.

For an approximate insight into the vehicle cornering dynamics a simplified vehicle model can be employed. A simple plane model consists of two masses representing the vehicle's sprung and unsprung mass. The masses are coupled via a virtual suspension roll centre joint. Motion of both masses is restricted to the roll plane only. In Fig. 2 the roll plane model and representative parameters are shown.

When neglecting the motion dynamics, the equation describing the moment equilibrium around the zero-level centre point can be written as

$$(F_{z,r} - F_{z,l})\left(\frac{T}{2}\right)\cos\phi_u + (m_s h_{cg} + m_u h_u)A_y + m_s g(h_r \sin\phi_s + z_r \sin\phi_u) = 0 \tag{14}$$

From equation (14), the $LLT_B$ coefficient denoting the lateral load transfer in roll plane can be derived as

$$LLT_B = \frac{F_{z,r} - F_{z,l}}{(m_s + m_u)g} = \frac{-2[(m_s h_{cg} + m_u h_u)(A_y/g) + m_s(h_r \sin\phi_s + z_r \sin\phi_u)]}{T\cos\phi_u(m_s + m_u)} \tag{15}$$

Assuming small angles and neglecting the unsprung mass contribution ($m_s \gg m_u$), equation (15) can be further simplified to

$$LLT_B = \frac{2}{T}\left(h_{cg}\frac{A_y}{g} + h_r\phi_s + z_r\phi_u\right) \tag{16}$$

Equations (15) and (16) are still impractical for implementation. The implementation would require exact knowledge of the vehicle parameters and the vehicle states, which are subjected to variations;

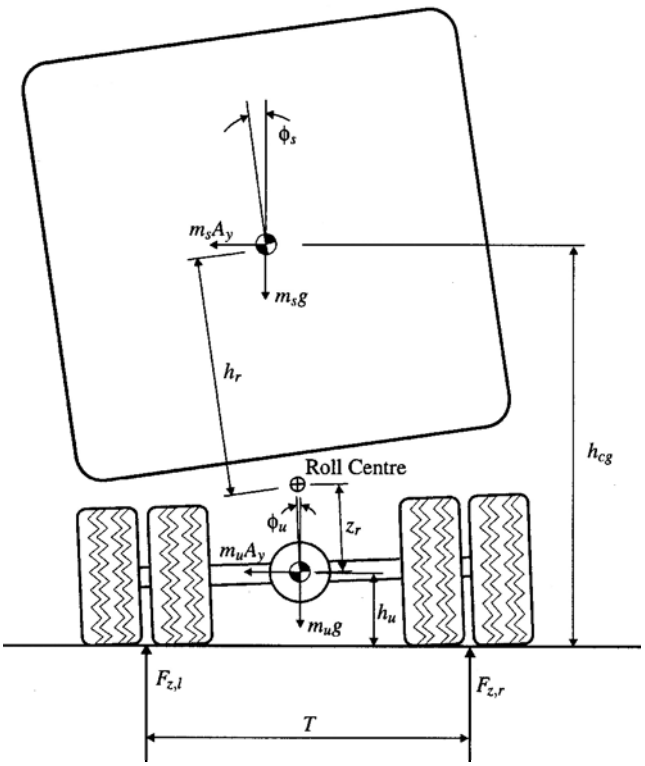


**Fig. 2** Simplified vehicle roll plane model

however, the equations demonstrate the LLT coefficient assessment complexity.

Following the Newton–Euler approach of analysing rigid-body motion dynamics, the roll motion dynamics of the trailer sprung mass can be described by the second-order differential equation

$$m_s g h_r \sin\phi_s + m_s h_r A_y \cos\phi_s - K_{\phi s}\phi_s - C_{\phi s}\dot{\phi}_s = (I_x + m_s h_r^2)\ddot{\phi}_s \quad (17)$$

where

$K_{\phi s}$ = total torsional stiffness of the suspension
$C_{\phi s}$ = total torsional damping of the suspension
$I_x$ = mass moment of inertia determined according to the trailer longitudinal axis

Similarly, the equation describing the unsprung mass motion can be derived. In this case, it is reasonable to neglect the unsprung mass inertial contributions:

$$(F_{z,r} - F_{z,l})\frac{T}{2} = K_{\phi s}\phi_s + m_s z_r A_y \quad (18)$$

Equation (18) is in essence valid for each vehicle axle. The difference exists only in the portion of the sprung mass that is supported by a particular axle (this will be denoted as a product $m_s q$) and in particular roll stiffness. If the trailer axles are considered as the rear unsprung lumped mass and the tractor drive axles as the front unsprung lumped mass then the static normal loading of these axles can be approximated, accounting for the load transfer along the vehicle longitudinal axis. Thus, the normal loading of the trailer axles when neglecting the unsprung mass is

$$F_{z,\text{rear}} = m_s q_{\text{rear}} = m_s\left(\frac{L_{B,f}}{L_B}g + \frac{h_{cg}}{L_B}A_x\right) \quad (19)$$

In the above equation, parameters $L_{B,f}$ and $L_{B,r}$ geometrically determine the longitudinal load distribution on the trailer (see Fig. 1). $L_B$ is a trailer wheel base and $A_x$ is a longitudinal acceleration. When considering the load of the tractor drive axles, the tractor mass contribution needs to be incorporated. The contributions of the trailer and tractor sprung masses are then summed as

$$F_{z,\text{front}} = m_s q_{\text{front}} = m_s\left(\frac{L_{B,r}}{L_{B,f}+L_{B,r}}g - \frac{h_{cg}}{L_{B,r}+L_{B,f}}A_x\right) + m_A\left(\frac{L_{A,f}}{L_{A,f}+L_{A,r}}g + \frac{h_{cg,A}}{L_{A,f}+L_{A,r}}A_x\right) \quad (20)$$

where

$m_A$ = tractor mass
$L_{A,f}$ and $L_{A,r}$ = tractor longitudinal c.g. positions
$L_A$ = tractor wheel base
$h_{cg,A}$ = tractor c.g. height

Obeying equations (18), (19) and (20), the terms defining the lateral load transfers $\text{LLT}_A$ and $\text{LLT}_B$ can be derived:

$$\text{LLT}_A = \frac{F_{z,r} - F_{z,l}}{F_{z,\text{front}}} = \frac{2\{A_x A_y(-h_{cg}L_A m_s + h_{cg,A}L_B m_A)z_r + g[K_{\phi s,f}L_B L_A\phi_s + A_y(L_{B,r}L_A m_s + L_{A,f}L_B m_A)z_r]\}}{g(L_{B,r}gL_A m_s - A_x h_{cg}L_A m_s + L_{A,f}gL_B m_A + A_x h_{cg,A}L_B m_A)T} \quad (21)$$

$$\text{LLT}_B = \frac{F_{z,r} - F_{z,l}}{F_{z,\text{rear}}} = \frac{2gK_{\phi s,r}L_B\phi_s + 2L_{B,f}A_y g m_s z_r + 2A_x A_y h_{cg} m_s z_r}{L_{B,f}g^2 m_s T + A_x g h_{cg} m_s T} \quad (22)$$

In equations (21) and (22) the influence of the vehicle articulation is neglected as unimportant, and the lateral and vertical accelerations ($A_y$, $A_z$) are expressed in the inertial coordinate system. However, in real operation, the orientation of the accelerometers mounted to the trailer is changing in accordance with the sprung mass roll angle $\phi_s$. Hence, the transformation between the inertial ground-based and the trailer body-based coordinate systems is needed in order to relate the measured values ($a_y$, $a_z$) with inertial accelerations:

$$a_y = A_y\cos\phi_s + g\sin\phi_s$$
$$a_z = -A_y\sin\phi_s + g\cos\phi_s \quad (23)$$

### 3.2.1 *Construction of the extended Kalman filter*

An extended Kalman filter [**21**] is used to estimate the $\text{LLT}_B$ coefficient and vehicle state histories. The estimation model combines the relations (17), (21), (22) and (23). The model is represented by a non-linear state-space description incorporating state and measurement difference equations:

$$\boldsymbol{x}_{k+1} = \boldsymbol{f}(\boldsymbol{x}_k, \boldsymbol{u}_k, \boldsymbol{w}_k)$$
$$\boldsymbol{z}_k = \boldsymbol{h}(\boldsymbol{x}_k.\, \boldsymbol{v}_k) \quad (24)$$

In equations (24) the non-linear function $\boldsymbol{f}$ relates the state vector $\boldsymbol{x}$ and the input vector $\boldsymbol{u}$ at time step $k$ to the state at step $k+1$. The measurement vector $\boldsymbol{h}$ relates the state to the measurements $\boldsymbol{z}_k$. Vectors $\boldsymbol{w}_k$ and $\boldsymbol{v}_k$ denote the superimposed process and measurement noise respectively. The state vector $\boldsymbol{x}_k$ is defined as

$$\boldsymbol{x}_k = [\phi_s\ \dot{\phi}_s\ A_x\ \dot{A}_x\ A_y\ \dot{A}_y\ \text{LLT}_B\ \dot{\text{LLT}}_B\ \ddot{\text{LLT}}_B\ \text{LLT}_A\ \dot{\text{LLT}}_A\ \ddot{\text{LLT}}_A]^T$$

The particular functions of the state equation are then

given as

$$\begin{bmatrix} f_1 \\ f_2 \\ f_3 \\ f_4 \\ f_5 \\ f_6 \\ f_7 \\ f_8 \\ f_9 \\ f_{10} \\ f_{11} \\ f_{12} \end{bmatrix} = \begin{bmatrix} \dot{\phi}_s \\ (m_s g h_r \sin\phi_s + m_s h_r A_y \cos\phi_s - K_{\phi s}\phi_s - C_{\phi s}\dot{\phi}_s)/(I_x + m_s h_r^2) \\ \dot{A}_x \\ 0 \\ \dot{A}_y \\ 0 \\ \dfrac{2gK_{\phi s,r}L_B\phi_s + 2L_{B,f}A_y g m_s z_r + 2A_x A_y h_{cg} m_s z_r}{Ag^2 m_s T + A_x g h_{cg} m_s T} \\ \mathrm{L\ddot{L}T_B} \\ 0 \\ \mathrm{L\dot{L}T_A} \\ \mathrm{L\ddot{L}T_A} \\ 0 \end{bmatrix} \tag{25}$$

The measurement vector $\boldsymbol{z}_k = [\dot{\phi}_s \ a_x \ a_y \ a_z \ \mathrm{LLT_A}]^T$ incorporates all measurement values. The non-linear measurement equation, which incorporates the sprung mass roll rate, three-dimensional trailer acceleration and the $\mathrm{LLT_A}$ coefficient, then takes the form

$$\begin{bmatrix} h_1 \\ h_2 \\ h_3 \\ h_4 \\ h_5 \end{bmatrix} = \begin{bmatrix} \dot{\phi}_s \\ A_x \\ A_y \cos\phi_s + g\sin\phi_s \\ -A_y \sin\phi_s + g\cos\phi_s \\ \dfrac{2\{A_x A_y(-h_{cg}L_A m_s + h_{cg,A}L_B m_A)z_r + g[K_{\phi s,f}L_B L_A \phi_s + A_y(L_{B,r}L_A m_s + L_{A,f}L_B m_A)z_r]\}}{g(L_{B,r}gL_A m_s - A_x h_{cg}L_A m_s + L_{A,f}gL_B m_A + A_x h_{cg,A}L_B m_A)T} \end{bmatrix} \tag{26}$$

The discrete-time extended Kalman filter (EKF) algorithm is implemented as adopted from reference [**22**]. The EKF measurement update equations are shown below:

$$\mathbf{K}_k = \mathbf{P}_k^- \mathbf{H}_k^T (\mathbf{H}_k \mathbf{P}_k^- \mathbf{H}_k^T + \mathbf{R}_k)^{-1} \tag{27}$$

$$\hat{\boldsymbol{x}}_k = \hat{\boldsymbol{x}}_k^- + \mathbf{K}(\boldsymbol{z}_k - \boldsymbol{h}(\hat{\boldsymbol{x}}_k^-, 0)) \tag{28}$$

$$\mathbf{P}_k = (\mathbf{I} - \mathbf{K}_k \mathbf{H}_k)\mathbf{P}_k^- \tag{29}$$

while the EKF time update equations are as follows:

$$\mathbf{P}_{k+1}^- = \mathbf{A}_k \mathbf{P}_k \mathbf{A}_k^T + \mathbf{Q}_k \tag{30}$$

$$\hat{\boldsymbol{x}}_{k+1}^- = \boldsymbol{f}(\hat{\boldsymbol{x}}_k, \boldsymbol{u}_k, 0) \tag{31}$$

Equations (27) to (31) form the complete set of equations for the EKF algorithm. The EKF propagates the state and error covariance estimates (31) and (30) by computing the filter gain matrix (27) and by updating the state and covariance estimates based on the measurement residuals (28) and (29). Matrices $\mathbf{A}_k$ and $\mathbf{H}_k$ are computed by linearizing equations (24) around $\hat{\boldsymbol{x}}_k^-$ at each time step. Matrix $\mathbf{A}$ is thus the Jacobian matrix of partial derivatives of $\boldsymbol{f}(\,)$ with respect to $\boldsymbol{x}$:

$$\mathbf{A}_k = [A_{ij}] = \frac{\partial f_i}{\partial x_j}(\boldsymbol{x}_k, \boldsymbol{u}_k, 0) \tag{32}$$

and matrix $\mathbf{H}$ is the Jacobian matrix of partial derivatives of $\boldsymbol{h}(\,)$ with respect to $\boldsymbol{x}$:

$$\mathbf{H}_k = [H_{ij}] = \frac{\partial h_i}{\partial x_j}(\boldsymbol{x}_k, 0) \tag{33}$$

The filter is initialized with a state estimate corresponding to the true state and a large covariance matrix. Figure 3 offers a complete picture of the EKF operation.

## 4 EVALUATION OF THE LLT ESTIMATION ALGORITHM

The proposed LLT coefficient estimation method was evaluated by the advanced vehicle computer simulation system CASCADE. The CASCADE (computer aided simulator of car, driver and environment) vehicle simulator was developed by the DaimlerChrysler Corporation (DaimlerChrysler, GmbH, Germany) to facilitate studies of the dynamic behaviour of large commercial vehicles. CASCADE is an integrated set of computer tools implemented in the Matlab/Simulink environment. It solves the equations of motion numerically to predict three-dimensional forces and motions of a vehicle in response to braking and steering inputs.

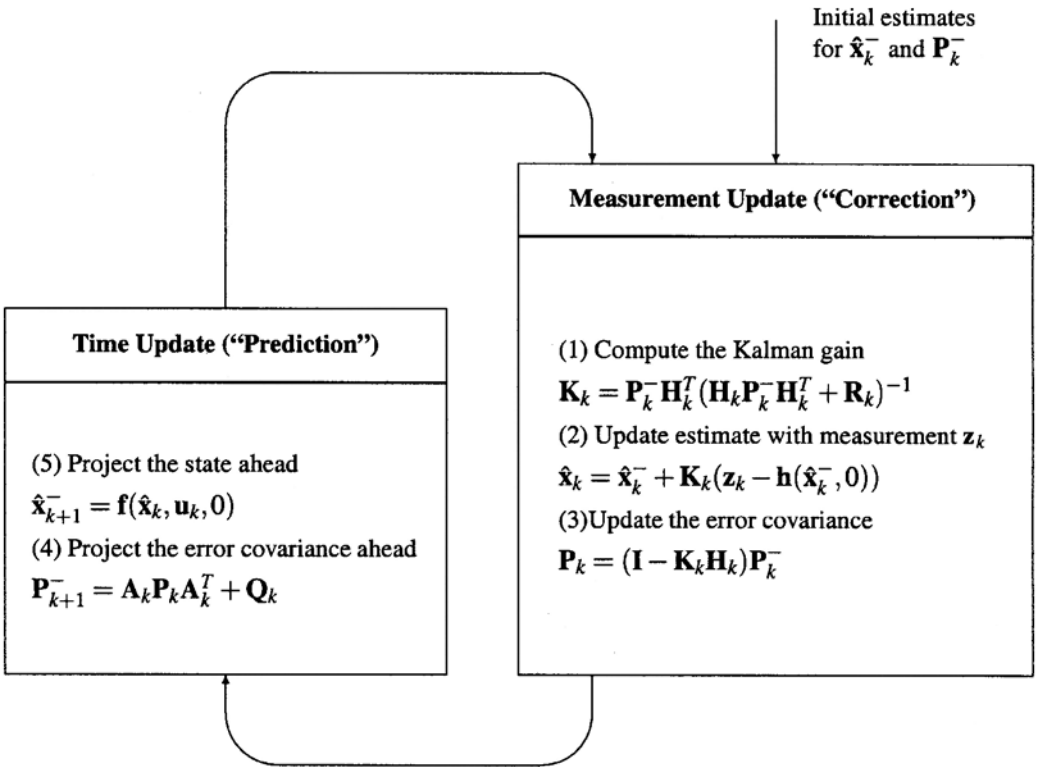


**Fig. 3** A complete picture of the extended Kalman filter operation

CASCADE uses detailed non-linear tyre models and non-linear spring models, and includes the major kinematic and compliance effects in the suspensions and steering systems in trucks. The kinematical and dynamical equations are valid for full non-linear three-dimensional motions of rigid bodies. For control inputs, CASCADE accepts time histories of brack/acceleration inputs and the steering wheel angle. The simulation results are available as three-dimensional graphic animation and as plots of output variables. Vehicle parameters are accessible in initialization text files. In the present project, the simulator was configured to model the dynamics of a Freightliner Century Class A12329 tractor/trailer with a 53 foot (16.15 m) trailer. In Fig. 4 the picture frames from the animation output are presented when the truck is performing the double-lane change manoeuvre. In animation, the tyre–road contact forces under each wheel are illustrated by solid lines. Graphs below show the vertical wheel loadings for each vehicle side and the lateral load transfer of the tractor and the trailer. Vertical dashed lines denote the time instants of illustrated motion sequences.

The lateral load transfer estimation algorithm was evaluated with two test driving manoeuvres. As a first test, the spiral manoeuvre was chosen as the last demanding task. During cornering with linearly increasing vehicle yaw angle, the dynamic contributions are absent and thus the system behaves as in quasi-static mode. As a second test, the double-lane change manoeuvre was chosen as the most demanding manoeuvre, where the dynamic contributions play an important role. In the top half of Fig. 5 the steering inputs in the form of desired vehicle yaw angle are presented for both test manoeuvres. The resulting motion trajectories are presented in the figures below, describing the motion of the tractor front and the trailer rear axles.

The evaluation was accomplished on a series of simulation runs with an integration step of 0.001 s and duration of 15 s. Before further processing, the output data were downsampled to 0.1 s. Eleven different loading conditions with variations in mass properties and load positions were tested in manoeuvres performed with four different forward velocities: 40, 60, 80 and 100 km/h. In this way, a wide range of truck operational conditions was covered. The parameters of loading conditions are listed in Table 1. In the table the inertial parameters are valid for the payload and trailer together. Vector $(r_x, r_y, r_z)$ describes the loaded trailer c.g. position and is defined relative to the centre ground point in the middle of the tractor driving axles (point O in Fig. 1). Thus, the distances $r_x$ and $r_z$ correspond to the parameters $L_{\mathrm{B,f}}$ and $h_{\mathrm{cg}}$ respectively. The distance $r_y$ denotes the lateral displacement of the c.g. position from the centre of the trailer. For all simulation runs, the values of the parameters, meaningful for the LLT estimation algorithm, were fixed and were assessed as they are collected in Table 2. For the characterization of estimation performance, the root mean square (r.m.s.) error between the actual and the estimated LLT outputs was calculated as an indication of how strongly the outputs

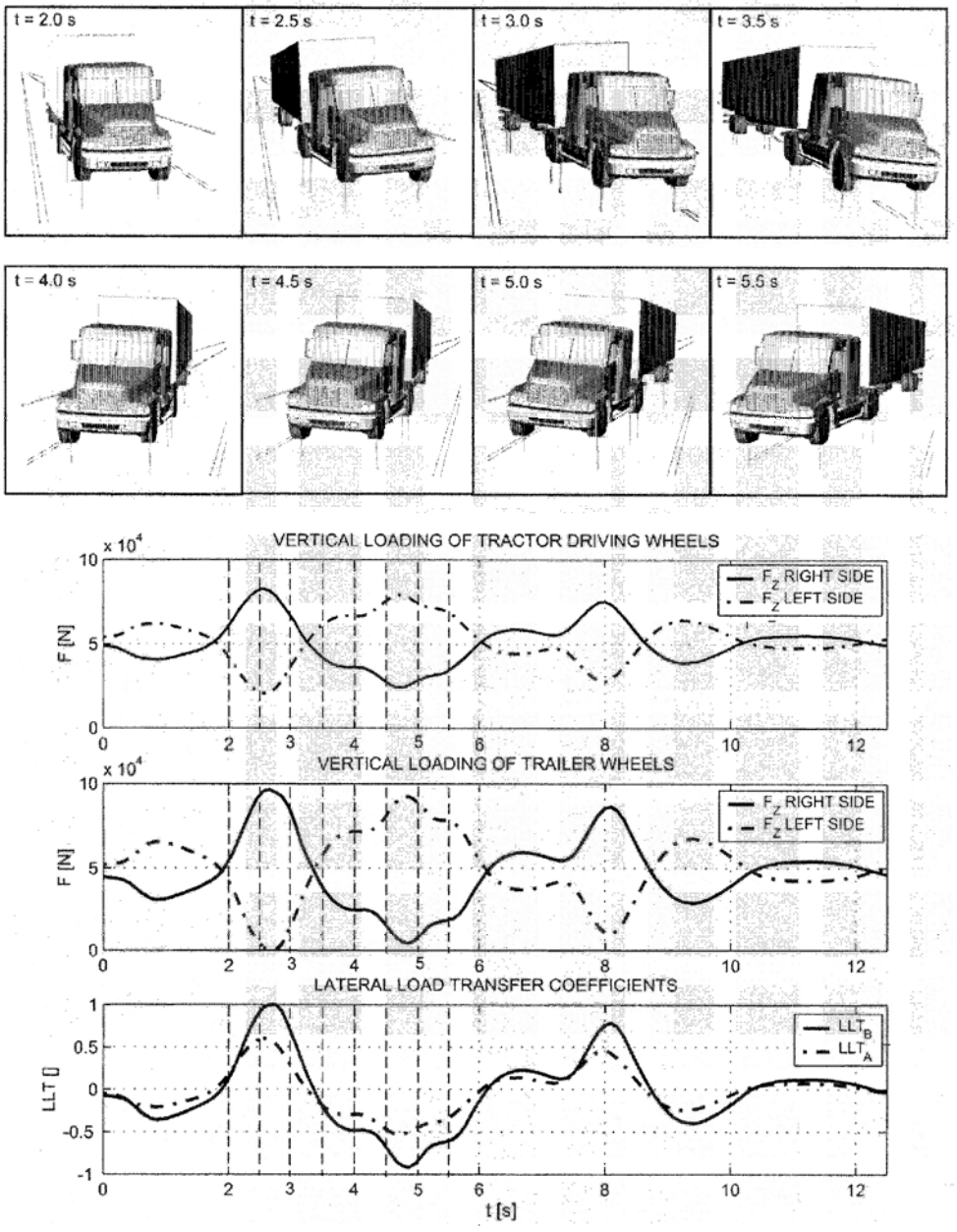


**Fig. 4** Double-lane change manoeuvre of the Freightliner Century Class heavy freight vehicle simulated by the CASCADE software package

are correlated. The smaller the r.m.s. error the stronger is the correlation and the better the estimation performance.

## 5 RESULTS

The performance of the LLT estimation algorithm was characterized by the r.m.s. error coefficient between the actual and estimated $LLT_A$ and $LLT_B$ values. The r.m.s. error results are presented for a range of operating conditions in two bar graphs. The graphs demonstrate the estimation performance for the tractor and the trailer separately. Additionally, for each test manoeuvre, two examples are chosen and the $LLT_A$ and $LLT_B$ time courses are presented. The examples are chosen in a way to demonstrate good and worse case estimation performances.

In Fig. 6, two bar graphs represent the r.m.s. error results for the LLT estimation achieved during the spiral manoeuvre. In Fig. 7, for the spiral manoeuvre, two estimation examples are given. On the left, the time courses for the $LLT_A$ and $LLT_B$ are presented, demonstrating a good performance example. These results were achieved with full loading and 80 km/h forward velocity. On the right side of the figure, the worse case performance example is given, presenting the time courses achieved with upward loading and 80 km/h forward velocity.

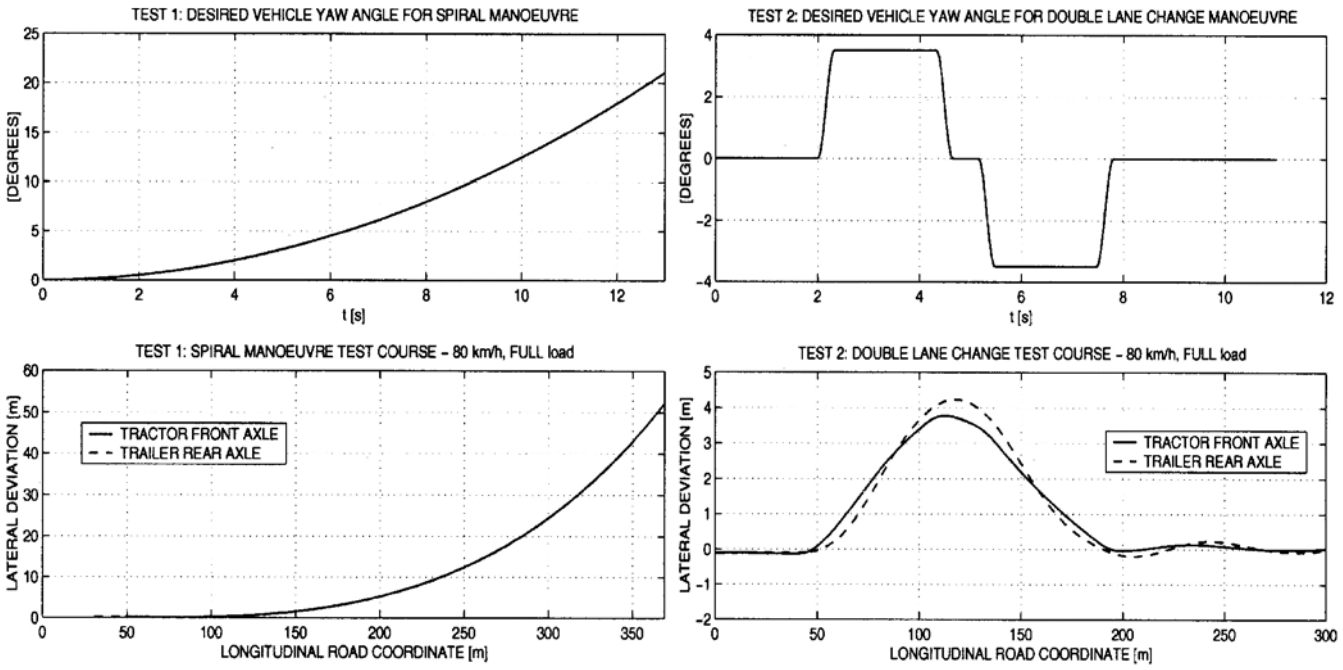


**Fig. 5** Steering inputs and resulting lateral deviations of the axle centre points in spiral and double-lane change manoeuvres

**Table 1** Evaluated loading conditions of the Freightliner heavy freight vehicle

| Loading | $m_s$ (kg) | $I_x$ (kg m$^2$) | $r_x \equiv L_{B,f}$ (m) | $r_y$ (m) | $r_z \equiv h_{cg}$ (m) |
|---|---|---|---|---|---|
| Full | 26 561 | 30 655 | 6.61 | 0 | 2.74 |
| Forward | 26 561 | 30 655 | 6.15 | 0 | 2.74 |
| Backward | 26 561 | 30 655 | 7.28 | 0 | 2.74 |
| Upward | 26 561 | 30 655 | 6.61 | 0 | 3.14 |
| Downward | 26 561 | 30 655 | 6.61 | 0 | 2.44 |
| Leftward | 26 561 | 30 655 | 6.61 | 0.3 | 2.74 |
| Rightward | 26 561 | 30 655 | 6.61 | −0.3 | 2.74 |
| 3_4 | 21 091 | 24 340 | 6.61 | 0 | 2.74 |
| Half | 16 016 | 18 480 | 6.61 | 0 | 2.74 |
| Quart | 10 743 | 12 400 | 6.61 | 0 | 2.74 |
| No | 5 470 | 6 310 | 6.61 | 0 | 2.74 |

**Table 2** Estimation algorithm parameters valid in all simulation runs

| | | |
|---|---|---|
| $c_1 = -0.50$ | $K_{\phi s} = 2\,314\,230$ N m/deg | $h_{cg} = 2.74$ m |
| $c_2 = 44.80$ | $C_{\phi s} = 42\,038$ N m s/deg | $h_r = 1.997$ m |
| $c_3 = -24.80$ | $K_{\phi s,f} = 947\,991$ N m/deg | $L_B = 13$ m |
| $r_0 = 0.51$ m | $K_{\phi s,r} = 1\,366\,239$ N m/deg | $L_{B,f} = 7$ m |
| $T = 1.83$ m | $I_x = 30\,655$ kg m$^2$ | $L_{B,r} = 6$ m |
| $l_{A2} = 2.24$ m | $m_s = 25\,365$ kg | $L_A = 5.6$ m |
| $l_{A3} = 3.63$ m | $m_A = 7098$ kg | $L_{A,f} = 2.56$ m |
| $z_r = 0.75$ m | $h_{A,cg} = 0.91$ m | $L_{A,r} = 3.04$ m |

Similarly to the spiral manoeuvre, the results are given for the double-lane change manoeuvre. Two bar graphs in Fig. 8 present the r.m.s. error results for a range of operating conditions. Bars denoted by the capital R represent the examples where the simulation run resulted in a rollover state. Two examples in Fig. 9 demonstrate the good and worse case examples. Estimation graphs on the left were achieved with full loading and 80 km/h, while estimation graphs on the right were achieved with the same velocity but upward loading.

## 6 DISCUSSION AND CONCLUSIONS

The presented results confirm a robust operation of the lateral load transfer estimation without known wheel vertical loadings. A reliable operation is confirmed in static as well as in highly dynamic driving manoeuvring.

Good tracking performance is demonstrated for the tractor load transfer estimation. The proposed approach of the $LLT_A$ estimation exhibits a low variance over a broad operating range. The results prove that the averaged estimation accuracy for most loading conditions lies within the 95 per cent confidence interval. Slightly higher estimation errors are evident in double-lane change manoeuvres accomplished at higher vehicle forward velocities and lower payloads. Since the accuracy of the $LLT_A$ estimation depends on the assessment of wheel friction and slip, the errors can be attributed to the approximate model of tyre–road friction employed in this study. An advantage is that the method exhibits poorer estimation results in operating conditions where the vehicle has better roll stability. However, a more complex wheel friction model that would account for the influence of the drive velocity and wheel load would improve the estimation performances. In the system implementation on the real vehicle, the quality of the $LLT_A$ estimation will also be subjected to the wheel slip estimation error. In this work the wheel slip information

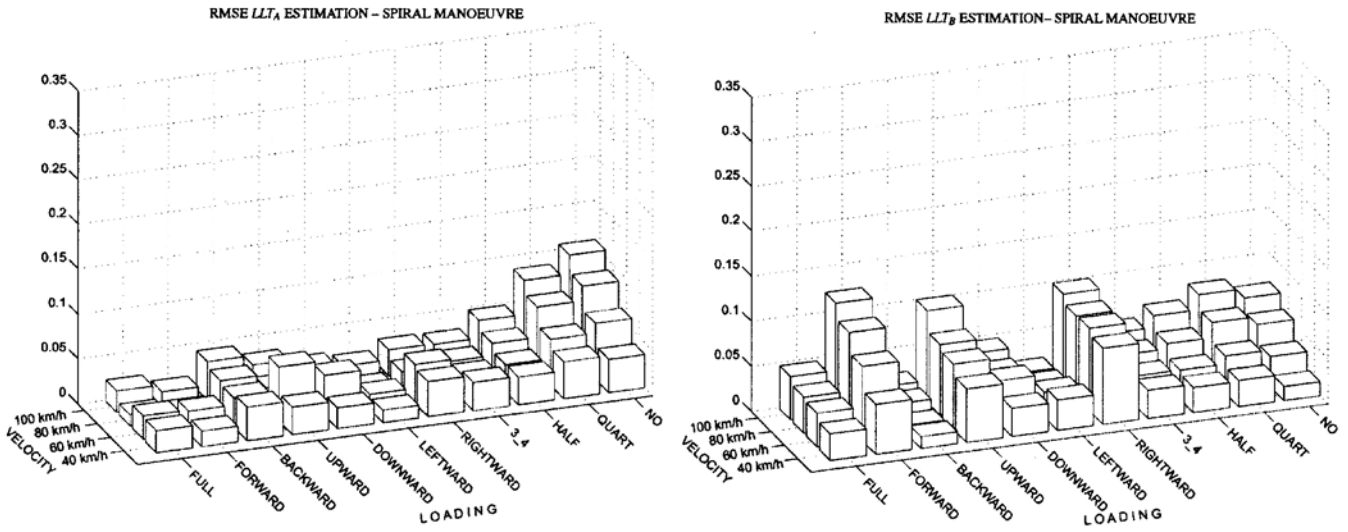


**Fig. 6** Root mean square error (RSME) evaluation results for the spiral manoeuvre: left, $LLT_A$ estimation; right, $LLT_B$ estimation

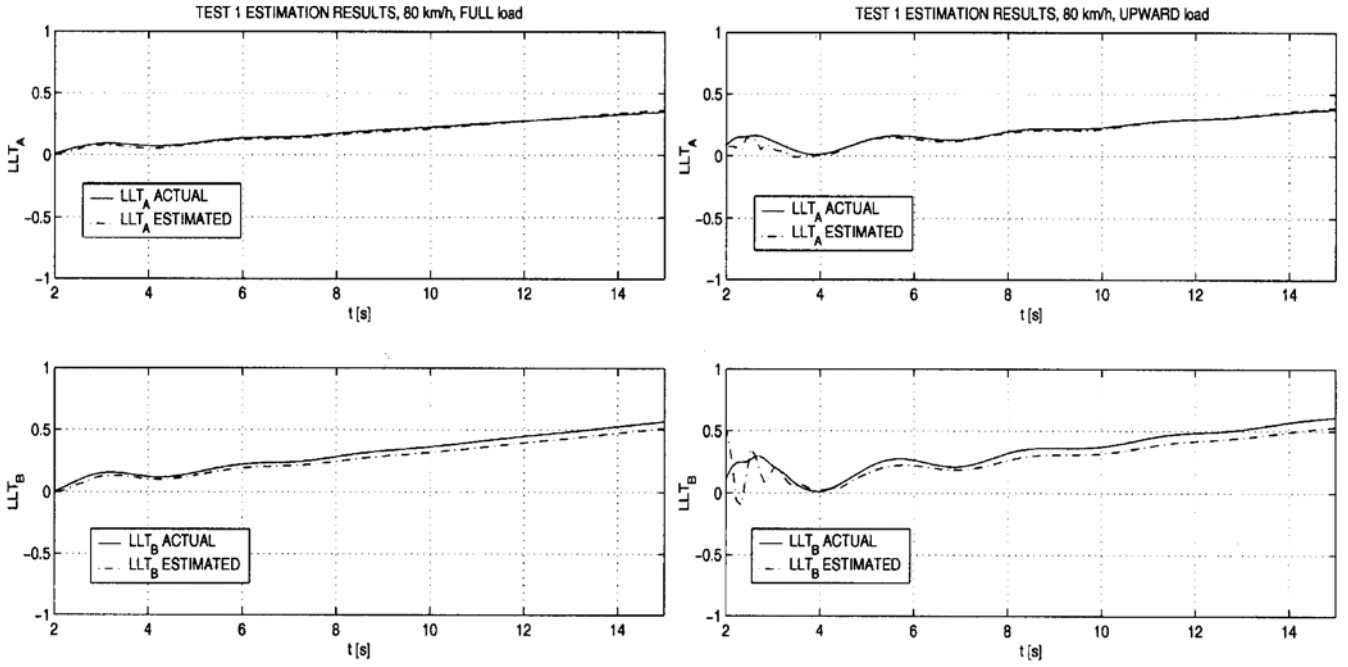


**Fig. 7** $LLT_A$ and $LLT_B$ estimation during the spiral manoeuvre: left, good case example; right, worse case example

was considered as being available on board and therefore its assessment error was beyond the scope of the study.

Slightly more variability to the operating conditions can be observed in the $LLT_B$ estimation results. It is demonstrated that the estimation algorithm is more sensitive to the load position than to the load mass. In addition, the system shows performance degradation when increasing the vehicle's forward velocity. However, for velocities up to 80 km/h (highway speed limit) the estimated states follow the actual state mostly within the 90 per cent confidence interval. From the results it is evident that the peaks of estimation error occur when the $LLT_B$ is changing the direction of its tendency. In these short intervals the vehicle roll behaviour is strongly influenced by dynamic effects. This implies that a more detailed dynamic model of the trailer unit implemented in the EKF algorithm would improve the estimation performances. Incorporation of the longitudinal compliance of the trailer and the non-linear behaviour of suspension into the model as well as on-line payload mass estimation are proposed for further system development. The oscillations of the estimated $LLT_B$, noticeable in Figs 7 and 9 at the beginning of the simulation tracks, can be attributed to the mismatch between the real and estimated

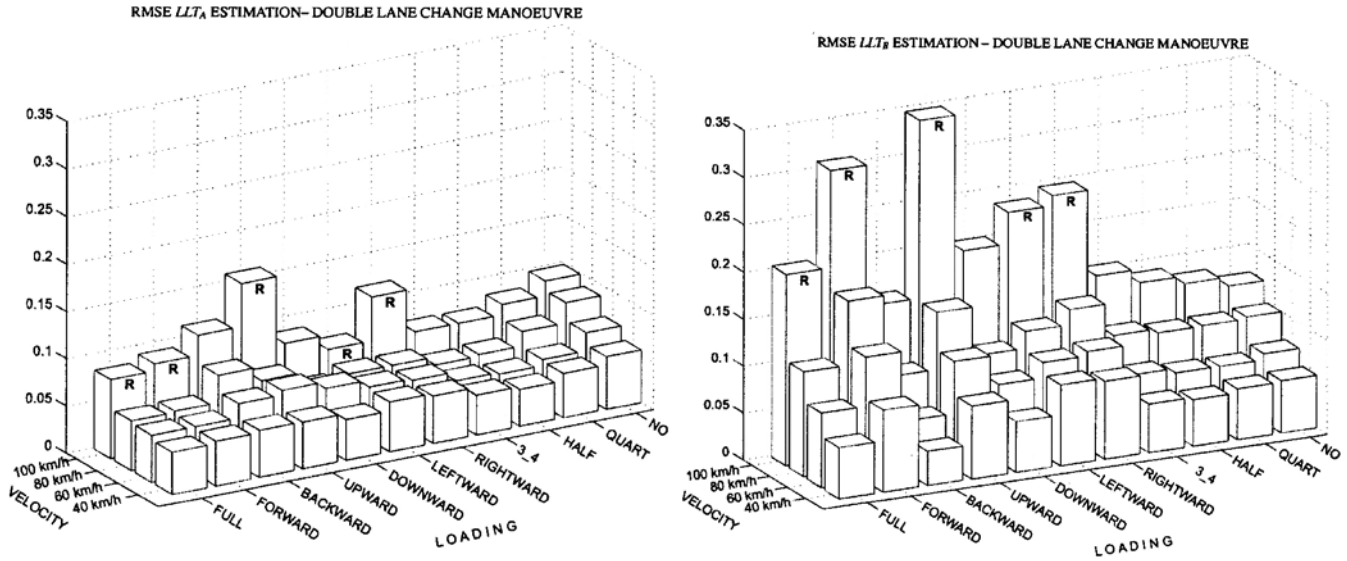


**Fig. 8** Root mean square error (RSME) evaluation results for the double-lane change manoeuvre: left, $LLT_A$ estimation; right, $LLT_B$ estimation

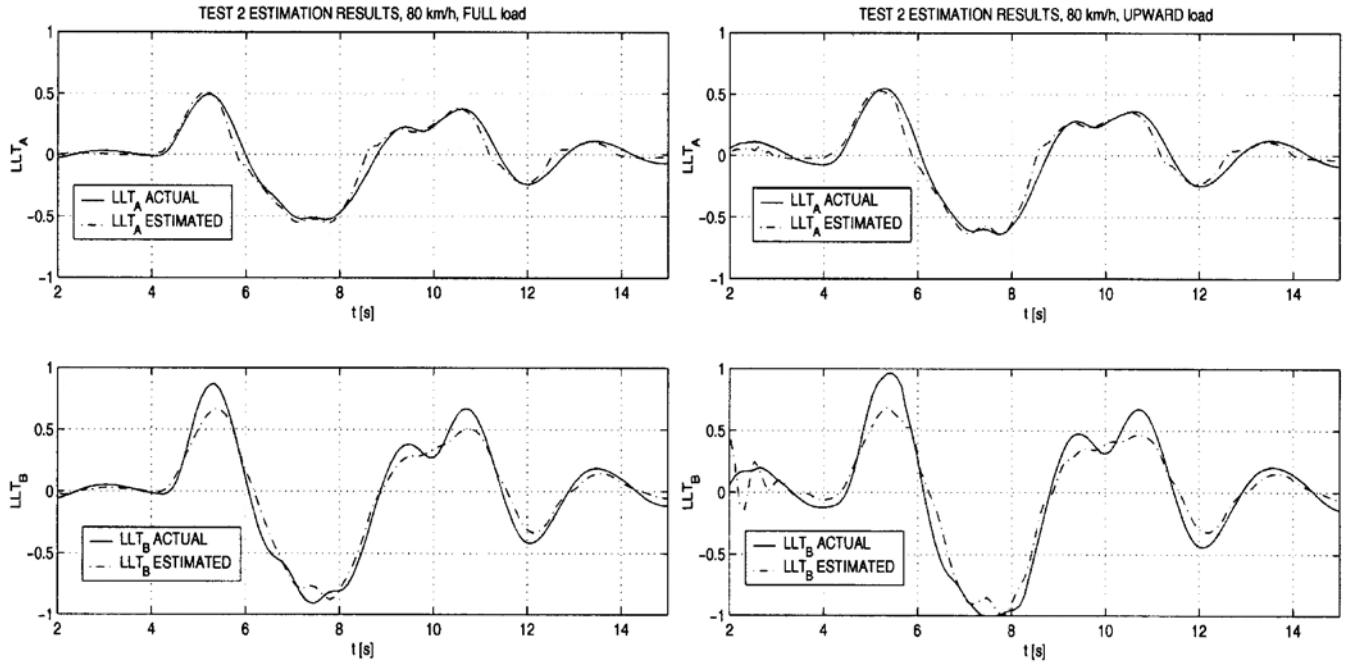


**Fig. 9** $LLT_A$ and $LLT_B$ estimation during the double-lane change manoeuvre: left, good case example; right, worse case example

initial states in the EKF. It can be observed that the oscillations are successfully damped out after a few seconds of EKF operation, thus not influencing the estimation accuracy in a long-term operation.

The methodology presented in this paper integrates two estimation procedures based on different physical presumptions and sensorics. The $LLT_A$ estimation procedure is aimed to run autonomously on a tractor unit without regards to the trailer type and loading. The $LLT_A$ signal obtained lacks some information about the whole vehicle lateral load transfer amplitude and phase, but with a safety reserve in consideration the $LLT_A$ estimation system could be used for an LLT approximation. As an extension providing a more accurate signal the $LLT_B$ estimation algorithm was developed. The algorithm is based upon the $LLT_A$ and trailer motion dynamics assessment. However, higher accuracy of obtained results requires implementation of additional sensors.

Sensor requirements for proper functioning of the estimation system are reasonable. The tractor load transfer is aimed to be estimated on the basis of sensory signals that are already incorporated in the vehicle control and

supervision systems, e.g. ABS. On the other hand, the trailer load transfer estimation is based on sensory information about the trailer acceleration and roll rate. In this simulation study, the trailer acceleration was acquired along three dimensions at a point in the trailer chassis level longitudinally displaced for 6.61 m from the trailer origin (point O in Fig. 1). The resulting values spanned $\pm 0.1g$, $\pm 0.4g$ and around $1g$ for longitudinal, lateral and vertical acceleration respectively. The roll angle rate was acquired at the same position with values spanned at $\pm 4$ deg/s. These results can serve as an orientation for determining the measuring ranges of sensors used in a real system. A sensory system integrating a three-dimensional accelerometer and a gyroscope seems to be the most practical choice for implementation. The sensory unit can be mounted on the trailer chassis preferably near to its c.g. position. As a practical enhancement, the sensory unit can be connected to the cabin control unit via a wireless link.

Computation requirements suggest that the estimation algorithm can be implemented in real time. Estimated signals can thus be delivered on-line to the driver through video or acoustic media. It is also conceivable that the estimates would be available as feedback control signals. Such closed-loop rollover prevention controllers, which have not been practical previously, may be useful in the future to enhance vehicle stability and road safety.

## ACKNOWLEDGEMENTS

The authors wish to thank Mr Thomas H. Breivik, Dr Roderick Murray-Smith and Dr Michael Schinkel for their helpful comments and suggestions to the project.

## REFERENCES

1 **Liu, P. J., Rakheja, S.** and **Ahmed, A. K. W.** Dynamic rollover threshold of articulated freight vehicles. *Heavy Vehicle Systems, Int. J. Veh. Des.*, 1998, **5**(3/4), 300–322.
2 **Swinson, D. B.** Vehicle rollover. *The Physics Teacher*, 1995, **33**(6), 360–366.
3 **Preston-Thomas, J.** and **El-Gindy, M.** Static rollover thresholds of heavy trucks. In Proceedings of the CSME, Forum SCGM 1992 on *Transport 1992+*, Montreal, Canada, 1992, pp. 946–951.
4 **Winkler, C. B.** and **Fancher, P. S.** A rationale for regulating roll stability of combination vehicles. In Proceedings of 3rd International Symposium on *Heavy Vehicle Weights and Dimensions*, Queens College, Cambridge, 1992, pp. 323–330.
5 **Lozia, Z.** Rollover thresholds of the biaxial truck during motion on an even road. *Veh. System Dynamics Suppl.*, 1998, **28**, 735–740.
6 **Ranganathan, R.** Rollover threshold of partially filled tank vehicles with arbitrary tank geometry. *Proc. Instn Mech. Engrs, Part D: J. Automobile Engineering*, 1993, **207**(D3), 241–244.
7 **Winkler, C. B., Ervin, R. D.** and **Hagan, M. R.** On-board estimation of the rollover threshold of tractor semitrailers. *Veh. System Dynamics*, 1999, **33**, 540–551.
8 **Hutchinson, G.** Large-truck properties and highway design criteria. *J. Transpn Engng*, 1988, **116**(1), 1–22.
9 **El-Gindy, M.** An overview of performance measures for heavy commercial vehicles in North America. *Int. J. Veh. Des.*, 1995, **16**(4/5), 441–463.
10 **Rakheja, S.** and **Piché, A.** Development of directional stability criteria for an early warning safety device. SAE Technical paper 902265, 1990.
11 **Verma, M. K.** and **Gillespie, T. D.** Roll dynamics of commercial vehicles. *Veh. System Dynamics*, 1980, **9**(1), 1–17.
12 **Liu, P. J., Rakheja, S.** and **Ahmed, A. K. W.** Detection of dynamic roll instability of heavy vehicles for open-loop rollover control. In Proceedings of the 1997 International Truck and Bus Meeting, SAE Special Publications 1308, Cleveland, Ohio, 1997, SAE paper 973263, pp. 105–112.
13 **Nalecz, A. G., Bindemann, A. C.** and **Brewer, H. K.** Dynamic analysis of vehicle rollover. In Proceedings of the 12th International Technical Conference on *Experimental Safety Vehicles*, 1989, Gottenburg, Sweden, pp. 803–819.
14 **Lund, Y. I.** and **Bernard, J. E.** Analysis of simple rollover metrics. SAE Technical paper 950306, 1995.
15 **Garrott, R. W.** and **Heydinger, G. J.** An investigation, via simulation, of vehicle characteristics that contribute to steering maneuver induced rollover. SAE Technical paper 920585, 1992.
16 **Kiencke, U.** and **Lars, N.** *Automotive Control Systems*, 2000 (Springer-Verlag, Berlin).
17 **Ray, L. R.** Nonlinear state and tire force estimation for advanced vehicle control. *IEEE Trans. Control System Technol.*, 1995, **3**(1), 117–124.
18 **Turco, P., Borodani, P.** and **Klaarenbeck, F. W. G.** Algorithms for a vehicle dynamics monitoring system based on model reference structure. *Meccanica*, 1997, **32**, 449–457.
19 **Venhovens, P. J. T. H.** and **Naab, K.** Vehicle dynamics estimation using Kalman filters. *Veh. System Dynamics*, 1999, **32**, 171–184.
20 **Schiffmann, J. K., Wallner, J. E.** and **Bhagwan, G. S.** Vehicle rollover sensing. US Pat. 6002975, 1999.
21 **Maybeck, P. S.** *Stochastic Models, Estimation, and Control*, 1989 (Academic Press, New York).
22 **Julier, S. J., Uhlman, J. K.** and **Durrant-Whyte, H. F.** A new approach for filtering nonlinear systems. In Proceedings of the 1995 American Control Conference, Seattle, Washington, 1995, pp. 1628–1632.